

Taming Multi-Domain, -Fidelity Data: Towards Foundation Models for Atomistic Scale Simulations

Tomoya Shiota,^{1,2,*} Kenji Ishihara,² Tuan Minh Do,² Toshio Mori,² and Wataru Mizukami^{1,2,†}

¹*Graduate School of Engineering Science, Osaka University,
1-3 Machikaneyama, Toyonaka, Osaka 560-8531, Japan*

²*Center for Quantum Information and Quantum Biology,
Osaka University, 1-2 Machikaneyama, Toyonaka 560-8531, Japan*

(Dated: December 18, 2024)

Machine learning interatomic potentials (MLIPs) are changing atomistic simulations in chemistry and materials science. Yet, building a single, universal MLIP – capable of accurately modeling both molecular and crystalline systems – remains challenging. A central obstacle lies in integrating the diverse datasets generated under different computational conditions. This difficulty creates an accessibility barrier, allowing only institutions with substantial computational resources – those able to perform costly recalculations to standardize data – to contribute meaningfully to the advancement of universal MLIPs. Here, we present Total Energy Alignment (TEA), an approach that enables the seamless integration of heterogeneous quantum chemical datasets almost without redundant calculations. Using TEA, we have trained MACE-Osaka24, the first open-source neural network potential model based on a unified dataset covering both molecular and crystalline systems, utilizing the MACE architecture developed by Batatia et al. This universal model shows strong performance across diverse chemical systems, exhibiting comparable or improved accuracy in predicting organic reaction barriers compared to specialized models, while effectively maintaining state-of-the-art accuracy for inorganic systems. Our method democratizes the development of universal MLIPs, enabling researchers across academia and industry to contribute to and benefit from high-accuracy potential energy surface models, regardless of their computational resources. This advancement paves the way for accelerated discovery in chemistry and materials science through genuinely foundation models for chemistry.

I. INTRODUCTION

Recent advances in machine learning interatomic potentials (MLIPs) have opened new opportunities in computational chemistry and materials science. Researchers can now perform atomistic simulations with nearly first-principles accuracy at orders of magnitude lower computational cost. [1–13] This paradigm shift has been propelled by increasingly sophisticated architectures—ranging from high-order equivariant neural networks to multi-scale graph neural representations—and an expanding wealth of large, first-principles-based datasets.[13–53] Inorganic-focused MLIPs now span much of the periodic table, making it easier to survey crystal structures and discover new phenomena in catalysis, semiconductor, and beyond. [54–67] At the same time, MLIPs for molecular systems have grown more versatile, achieving near hybrid density functional theory (DFT) accuracy across a range of organic, pharmaceutical, and biomolecular targets.[19, 23, 26, 47–49, 68–76]

Yet despite these advances, the pursuit of a truly “universal” MLIP—one that seamlessly unites the organic and inorganic realms—remains challenging. Molecular and crystalline datasets often differ in their computational methods, choice of DFT functionals, and ba-

sis sets, making their resulting potential energy surfaces (PESs) incompatible.[77–88] For example, inorganic datasets typically use plane-wave basis sets and generalized gradient approximations, while organic datasets rely on localized basis sets and hybrid functionals. Merging these heterogeneous sources – without recalculating vast portions of data – has been difficult, placing the development of foundation models in chemistry out of reach for many research groups with limited computational resources.

Here, we introduce a general strategy called Total Energy Alignment (TEA) that addresses this long-standing problem by harmonizing datasets generated under different computational settings. TEA uses a two-step approach—first aligning inner-core reference energies, then scaling atomization energies—to integrate datasets that previously could not be combined. Applying TEA to unify a large inorganic dataset (MPtrj)[57] and a broad organic set (OFF23[76], consisting of SPICE[47, 49], QMug[48], water clusters, and Tripeptides datasets), we have constructed MACE-Osaka24: a single open-source neural network potential capable of accurately modeling both organic molecular reactions and extended crystalline systems. Unlike previous multi-task approaches that simply switch between domains,[56, 89] MACE-Osaka24 handles organic and inorganic PESs with a single model. It not only outperforms specialized potentials in predicting reaction barriers for drug-like organic molecules, but also maintains state-of-the-art accuracy for inorganic systems.

* shiota.tomoya.ss@gmail.com

† mizukami.wataru.qiqb@osaka-u.ac.jp

This work has two key implications. First, by removing the need for costly recalculations, TEA helps democratize the creation of foundation models in chemistry, enabling research groups with limited computational resources to contribute more effectively. Second, MACE-Osaka24 shows that a single model can achieve high accuracy across both molecular and inorganic domains, suggesting a new level of interoperability. As data-driven discovery expands, the ability to seamlessly handle both organic and inorganic chemical spaces will accelerate catalyst design, functional material development, and the exploration of complex reactions. Together, the TEA framework and MACE-Osaka24 point the way toward truly universal MLIPs, enabling the next generation of foundation models to go beyond traditional domain boundaries.

The remainder of this paper is organized as follows. In Section II, we review related works on learning from datasets generated under different computational conditions. Section III introduces our TEA method, followed by details of the integrated datasets and the process of building multi-domain universal MLIPs. In Section IV, we assess the accuracy of the constructed multi-domain universal MLIP using a range of benchmarks: we compare predicted reaction barriers for organic molecules, evaluate lattice constants for inorganic crystals, and perform molecular dynamics simulations for liquid water. Section V discusses the implications of our findings and suggests directions for future research. Finally, we present our conclusions in Section VI.

II. RELATED WORKS

A goal of MLIPs has been to achieve first-principles accuracy in simulating chemical and materials systems while greatly reducing computational costs. Early methods, like Behler-Parrinello networks and Gaussian Approximation Potentials, showed that machine learning can reproduce high-level quantum chemistry results without directly solving the Schrödinger equation for every geometry.[12, 13] Since then, more advanced E(3)-equivariant graph neural networks and message-passing models have emerged, improving both accuracy and transferability.[15, 16, 18–20, 22–24] Concurrently, large-scale first-principles datasets—ranging from the Materials Project’s extensive inorganic databases[31, 32, 54, 57, 59] to molecular sets such as the QM9,[43] OFF23,[47–49, 76] and SPICE[47] datasets – have enabled the training of increasingly universal MLIPs. As a result, models such as MACE-MP-0[23, 59] and CHGNet[57] now approach state-of-the-art performance for inorganic crystals, while others, like MACE-OFF23[76] and AIMNet2,[72, 73] deliver high accuracy across diverse organic and biomolecular systems.

A major challenge in advancing universal MLIPs lies in the integration of these heterogeneous datasets – each constructed under different computational protocols, ba-

sis sets, and exchange-correlation functionals – into a single, cohesive training set. These differences affect reference energies, force field definitions, and whether the calculations include periodic conditions, making it hard to combine data directly.[77, 78] To date, several strategies have been attempted to bridge these discrepancies. For example, Δ -machine learning and multi-fidelity learning approaches learn corrections from lower- to higher-level references, allowing them to blend datasets at different accuracy levels. [90–93] However, these methods often need a reference dataset covering both fidelity/domain ranges and still face difficulties when data come from different software or fundamentally different computational setups. As a result, many solutions remain specialized to a specific domain, for example, to either molecular systems or periodic solids, but not both simultaneously.

When it comes to spanning organic and inorganic domains within a single MLIP, only a handful of attempts exist. For instance, PFP[56] uses multi-task learning to handle molecular and crystalline data together, but treats them as separate ‘modes’ rather than unifying their energy scales. Similarly, DPA-2[89] improves generalization by pretraining on multiple tasks—including molecules, crystals, and surfaces—but still depends on carefully managed workflows and fine-tuning, rather than directly merging heterogeneous datasets. These approaches highlight the advantages of multi-domain learning, such as better transferability, fewer data requirements, and stronger PES exploration. However, they have yet to solve the core issue of integrating data generated under different computational conditions into one consistent PES without extensive recalculations.

Another line of research has sought to align different datasets using physically meaningful reference values. For inorganic materials, methods like the Fitted Elemental Reference Energies (FERE) approach compare formation energies and elemental reference energies across various exchange-correlation functionals and calculation setups.[94–97] Recently, Gabellini et al.[52] introduced a large molecular dataset by converting total energies into atomization energies (analogous to formation energies), which helps reduce reliance on absolute reference values that differ among computational codes. However, atomization energies carry systematic errors depending on the computational protocol [98, 99]. As a result, simply transforming existing datasets into atomization energies does not guarantee more effective MLIP training. While these strategies offer promising leads, applying them to integrate large-scale organic and inorganic datasets – where both computational fidelity and the nature of the systems (extended solids vs. finite molecules) differ – remains non-trivial.

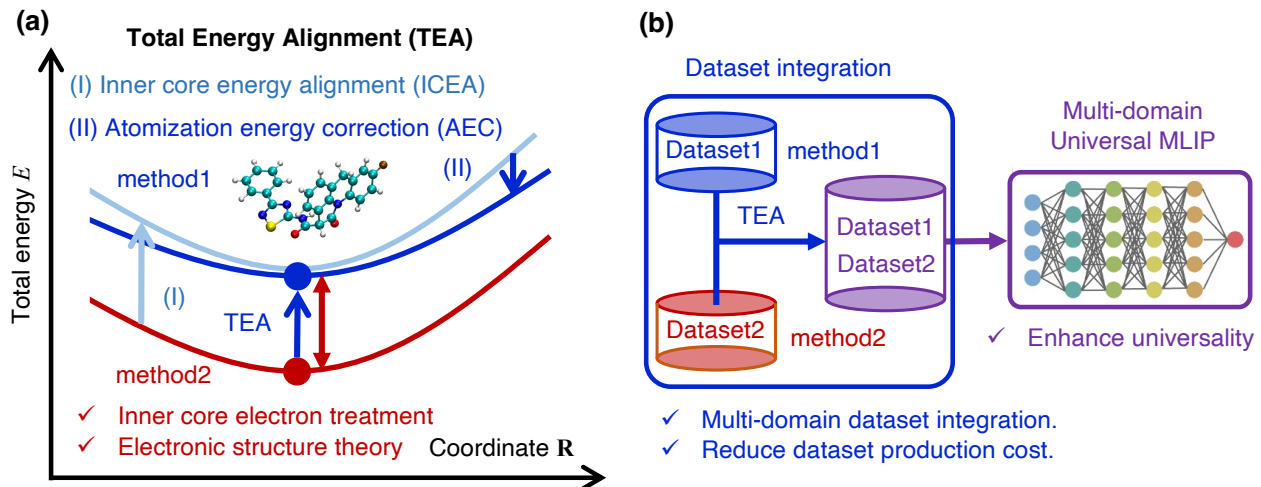


FIG. 1. (a) Comparison of total energies of a certain material computed by method 1 and 2, evaluated at coordinates obtained from method 2 as indicated by a double-headed arrow. Typical differences between the two methods include the treatment of inner core electrons, the choice of DFT functionals, and the electronic structure theories employed. The TEA technique developed in this study aligns the total energies from different methods to the reference energy of the target method. The arrows in the figure represent the two-step transformation of the potential energy surface (PES) through TEA, consisting of (I) inner core energy alignment (ICEA) and (II) atomization energy correction (AEC). (b) Schematic of the workflow illustrating how datasets generated by method 1 and method 2 are integrated using TEA. This integration enables the universal machine learning interatomic potential (MLIP) to be trained as a single task.

III. METHODS

A. Total Energy Alignment (TEA)

Developing a truly universal MLIP that can handle both molecular and extended solid systems requires a unified treatment of datasets generated under diverse computational conditions. However, merging these heterogeneous datasets directly is challenging because total energies are often not on a comparable scale. Here, we introduce the TEA framework, a two-step procedure designed to seamlessly reconcile datasets computed with different quantum chemical approaches, as illustrated in Fig. 1(a).

The TEA strategy consists of two key steps: (I) Inner Core Energy Alignment (ICEA) and (II) Atomization Energy Correction (AEC). ICEA corrects for systematic energy offsets caused by differences in treatments of core electrons, such as the use of effective core potentials or projector-augmented wave (PAW) methods, without altering relative energy differences. AEC subsequently scales atomization energies to account for discrepancies in computational fidelity, basis sets, or exchange-correlation functionals used across different datasets. By first aligning core-level energies and then applying a scalable correction to atomization energies, TEA provides a straightforward route to integrate previously incompatible datasets into a single, coherent training platform, as depicted schematically in Fig. 1(b).

1. Inner Core Energy Alignment (ICEA)

Different computational methods often treat inner-core electrons differently, which leads to systematic shifts in total energies. These differences do not usually affect chemical reactivity, but they hamper direct comparisons or combination of datasets. To address this, we first assume that relative quantities, such as atomization energies, remain consistent between two methods, denoted as method 1 and method 2.

For a system of N atoms, the atomization energy E_{at} is defined as:

$$E_{\text{at}} = \sum_{i=1}^N E_i^{P_i} - E_{\text{tot}}, \quad (1)$$

where $E_i^{P_i}$ is the energy of an isolated atom of species P_i , and E_{tot} is the total energy of the system.

If the atomization energies from method 1 and method 2 are equivalent,

$$E_{\text{at}}^{[1]} = E_{\text{at}}^{[2]}, \quad (2)$$

then the total energy from method 1 can be expressed in terms of method 2 as:

$$\begin{aligned} E_{\text{tot}}^{[1]} &= \sum_{i=1}^N E_i^{P_i, [1]} - E_{\text{at}}^{[1]} \\ &= \left(\sum_{i=1}^N E_i^{P_i, [1]} - \sum_{i=1}^N E_i^{P_i, [2]} \right) + E_{\text{tot}}^{[2]} \end{aligned} \quad (3)$$

This relation shows that we can shift the total energies from method 2 to match the reference scale of method 1 solely by using computed isolated-atom energies. In practice, ICEA sets a common baseline for both datasets, ensuring that differences arise from meaningful chemical effects rather than arbitrary computational choices.

2. Atomization Energy Correction (AEC)

After applying ICEA, certain residual differences in atomization energies still remain if the two datasets originate from different calculation protocols (e.g., distinct levels of theory, different basis sets, or contrasting exchange-correlation functionals). These differences manifest as systematic offsets that must be corrected before the datasets can be fully integrated.

We introduce a correction function f , relating the atomization energies of the two methods:

$$E_{\text{at}}^{[1]} = f\left(E_{\text{at}}^{[2]}\right). \quad (4)$$

To preserve simplicity and ensure robust performance, we adopt a single scaling factor a :

$$f\left(E_{\text{at}}^{[2]}\right) = a E_{\text{at}}^{[2]}. \quad (5)$$

In fact, previous studies have reported a linear relationship between the magnitude of the atomization energy and the systematic errors present [98, 99], making a simple scaling approach a practical choice.

This scaling guarantees that at equilibrium geometries, the energy landscapes align, making:

$$E_{\text{tot}}^{[1]} = \sum_{i=1}^N E_i^{P_i, [1]} - a E_{\text{at}}^{[2]}. \quad (6)$$

Because forces are gradients of the total energy, this correction consistently adjusts forces as well:

$$F_i^{[1]} = -\frac{\partial E_{\text{tot}}^{[1]}}{\partial \vec{r}_i} = -a \frac{\partial E_{\text{tot}}^{[2]}}{\partial \vec{r}_i} = a F_i^{[2]}. \quad (7)$$

This ensures that the entire potential energy surface is appropriately rescaled. Together, ICEA and AEC yield a coherent PES alignment that preserves relative energy differences and chemical accuracy across heterogeneous datasets.

B. Datasets

To demonstrate the effectiveness of TEA, we integrated two large-scale datasets: the MPtrj dataset, which provides inorganic structures calculated at the PBE[100] functional with plane-wave basis sets (PBE/PW) using Vienna Ab initio Simulation Package (VASP),[79–82] and the OFF23 dataset, an extensive organic dataset

computed at the ω B97M-D3(BJ)/def2-TZVPPD[101–104] level using Psi4.[85] Prior to integration, we remove the D3(BJ) dispersion correction from the OFF23 data to avoid double-counting dispersion effects in the final MLIP.

To determine the scaling factor a used in the AEC step and assess uncertainties, we also employed the QM9 dataset,[43] originally computed at B3LYP[105]/6-31G(2df,p) level using Gaussian09.[88] We recalculated QM9 using VASP (PBE/PW) and Psi4 (ω B97M-D3(BJ)/def2-TZVPPD) to generate QM9VASP and QM9Psi4 subsets, ensuring consistent reference points for establishing a . Full details of dataset preparation and integration, including corrections and final merged sets, are provided in Appendix VII A. The fully integrated organic-inorganic dataset is publicly available at <https://github.com/qiqb-osaka/mace-osaka24>.

C. MLIP Training

With TEA-enabled integration, we trained MLIPs using the MACE framework,[23, 59] specifically employing mace v0.3.6 (<https://github.com/ACEsuit/mace>). We leveraged the integrated MPtrj/OFF23 dataset after applying TEA, and refer to the resulting MLIP as MACE-Osaka24. The model and the final training data are available at <https://github.com/qiqb-osaka/mace-osaka24>.

Our training followed the hyperparameters, cost functions, and optimizers of MACE-MP-0-small and MACE-MP-0-large models described in Ref. [59], with a few modifications. For all models, we set a cutoff radius of 4.5 Å for constructing the atomic neighborhood graph. We used isolated atomic energies computed with spin polarization via VASP as references for the atomic species included in OFF23. Model training was performed using 32 A100 GPUs in parallel. Details of the MACE-Osaka24 model training procedure and hyperparameter settings can be found in Appendix VII B.

By unifying heterogeneous datasets under the TEA framework and leveraging advanced MLIP architectures, our approach yields a single universal potential model that can accurately describe both molecular and crystalline systems. This lays a critical foundation for accessible, high-fidelity PES modeling across the chemical and materials sciences.

IV. RESULTS

We evaluate the performance of the constructed multi-domain universal MLIPs, MACE-Osaka24-small and MACE-Osaka24-large. For comparison, we also performed simulations using MACE-MP-0 and MACE-OFF23, where feasible. Furthermore, we present simulation results obtained using other universal MLIPs, as

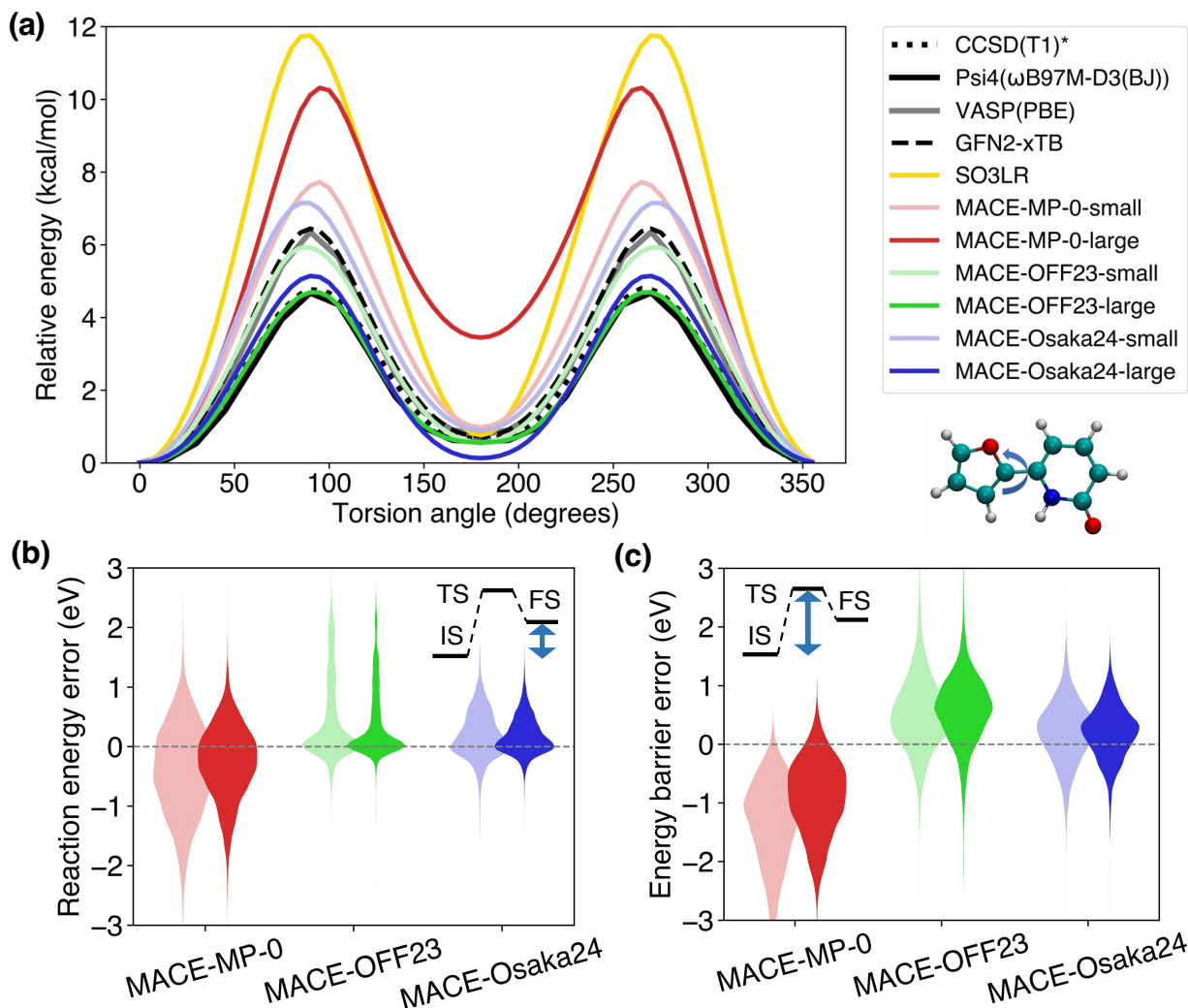


FIG. 2. (a) The optimized torsional potential energy surface (PES) of dihedral torsion in a representative organic molecule in biaryl torsion dataset [106] shown on the right side the figure, comparing results across various machine learning interatomic potentials (MLIPs), including SO3LR, MACE-MP-0, MACE-OFF23, and MACE-Osaka24 models, alongside reference calculations from Psi4 (ω B97M-D3(BJ)), VASP (PBE) and ORCA (CCSD(T1)*). The CCSD(T1)* values are taken from biaryl torsion benchmark [106]. (b) A violin plot of reaction energy errors, where the reaction energy is defined as the energy difference between the initial state (IS) and the final state (FS). The errors are calculated based on single-point energy calculations obtained using the MACE-MP-0, MACE-OFF23, and MACE-Osaka24 models, compared to single-point energy at the ω B97M-D3(BJ) level with Psi4 for the 10,073 organic reactions of Transition1x dataset. The results for small models are shown with lighter colors, while those for large models are shown with darker colors. (c) Violin plot of energy barrier errors, where the energy barrier is defined as the energy difference between the IS and transition state (TS), compared to single-point energy at the ω B97M-D3(BJ) level with Psi4 for the 10,073 organic reactions of Transition1x dataset for the same models as in (b), with lighter and darker colors representing small and large models, respectively.

well as DFT, and semiempirical and classical force fields, for additional reference.

First, we present the benchmark results for organic molecular systems. Table I shows the mean absolute errors (MAEs) of barrier heights for 78 drug-like biaryl torsions, compared against high fidelity reference energies at the coupled cluster level of theory provided in biaryl torsion benchmark[106]. Compared with the RMSEs in the benchmark by Kovács et al. [76], the approximately 0.1 kcal/mol difference in the accuracy of

MACE-OFF23 models is likely attributable to differences in the optimizer used for the torsional PES. Details of the biaryl torsion benchmark, including the computational settings for DFT and universal MLIPs, are described in Appendix VII C 3. The MACE-Osaka24-small and -large models achieved predictions that are 2.69 and 1.45 kcal/mol more accurate, respectively, compared to the predictions of MACE-MP-0-small and -large in torsion reactions of molecules. As shown in the study by Kovács et al. [76], the MACE-OFF23 models and

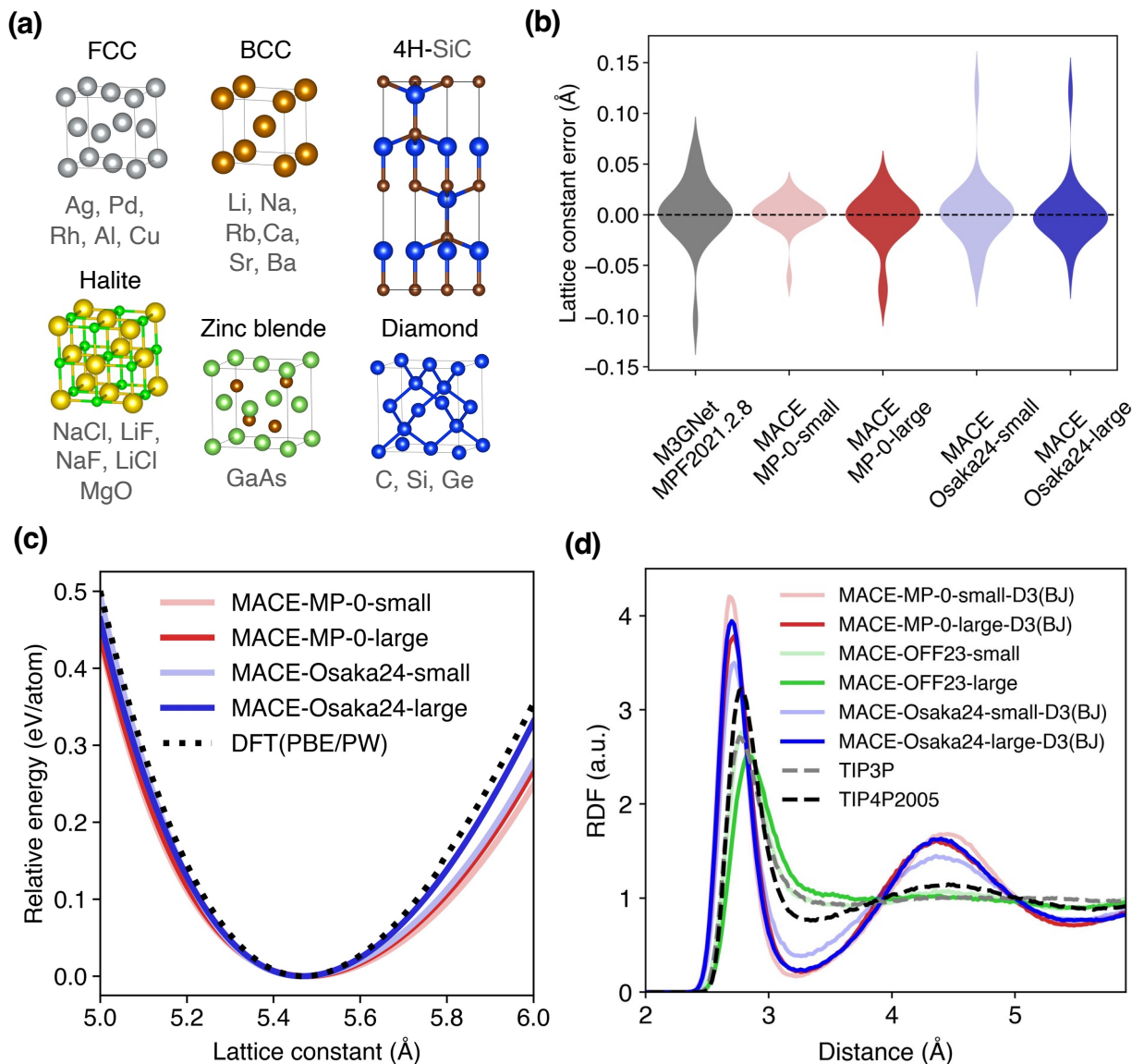


FIG. 3. (a) Crystal structures and their representative materials used in the lattice constant benchmark shown in (b): Face centered cubic (FCC) (e.g., Ag, Pd), body centered cubic (BCC) (e.g., Li, Na), Halite (e.g., NaCl), Zinc blende (e.g., GaAs), and Diamond (e.g., C, Si). (b) Violin plot showing the lattice constant error (Å) for different models, including MACE-MP-0-small, MACE-MP-0-large, MACE-Osaka24-small, MACE-Osaka24-large, and M3GNet trained on the MPF.2021.2.8 dataset. The errors are calculated with respect to lattice constants optimized using VASP with the PBE functional, employing the MPRelaxSet input provided by pymatgen from the Materials Project. (c) Relative energy (eV/atom) as a function of the lattice constant (Å) for Diamond Si crystal, predicted using MACE models (MP-0 and Osaka24 variants) and compared with VASP calculations. The VASP calculations at level were performed using the MPStaticSet input provided by pymatgen. (d) Radial distribution function (RDF, a.u.) for liquid water obtained from NVT simulations. Results are shown for MACE-MP-0 and MACE-Osaka24 models with D3(BJ) corrections, as well as for classical MD simulations using TIP3P and TIP4P/2005 force fields.

semiempirical GFN2-xTB [107] method provide quantitative predictions within chemical accuracy (1 kcal/mol) with respect to calculations at the level of coupled cluster theory. Similarly, our MACE-Osaka24 models also achieve chemical accuracy, demonstrating its effectiveness in providing precise predictions for molecular torsions. Fig. 2(a) shows the torsional PES of one of the

molecules in the biaryl torsion benchmark. The MACE-MP-0-large model overestimates the barrier height of the torsion reaction by about twice. Compared to the PES calculated at the PBE level using VASP, the difference is large. This result suggests that for MLIPs trained only on inorganic crystal domains, quantitative prediction of organic molecular domains is difficult. The MACE-

OFF23-small model gives predictions almost equivalent to the PBE level results. Our MACE-Osaka24-small model shows predictive performance almost equivalent to MACE-MP-0-small. The MACE-Osaka24-large model achieves predictive accuracy close to the high-fidelity ω B97M-D3(BJ), exceeding the predictive accuracy of the PBE level. These results suggest that learning datasets integrated by TEA allows the single model to inherit the accuracy of the original datasets.

Then, we evaluated the performance of universal MLIPs on the Transition1x dataset, focusing on their ability to predict reaction energies and energy barriers for 10,073 organic reactions. Details of the calculations are shown in Appendix VII C 4. Fig. 2(b) shows the distribution of reaction energy prediction errors, where MACE-Osaka24 achieved the lowest error spread compared to MACE-MP-0 and MACE-OFF23. Similarly, Fig. 2(c) highlights the performance on energy barrier prediction errors, indicating that MACE-Osaka24 consistently outperformed the other models, particularly in capturing transition state (TS) regions with higher accuracy. Table II quantitatively supports these observations. The MAEs for reaction energy predictions were 1.333 eV, 0.672 eV, and 0.457 eV for MACE-MP-0-small, MACE-OFF23-small, and MACE-Osaka24-small, respectively. The corresponding values for energy barrier predictions were 0.686 eV, 0.544 eV, and 0.336 eV. Larger models of each potential demonstrated further improvements, with MACE-Osaka24-large achieving the lowest MAEs: 0.404 eV for reaction energies and 0.265 eV for energy barriers. These results demonstrate that MACE-Osaka24, especially in its large model, offers superior predictive accuracy for both reaction energy and energy barrier predictions in the Transition1x dataset. This highlights the importance of tailored model architectures and training datasets that explicitly include transition state regions, enabling MLIPs to achieve high accuracy even for reactive systems far from equilibrium.

Next, we present the results of accuracy verification of universal MLIPs for crystalline systems listed in Fig. 3(a). The crystals used for the benchmark were those adopted in Section B.4 of the Supporting Information in the paper by Batatia et al [23]. Details of the calcula-

TABLE I. Mean absolute errors (MAEs) of barrier heights for 78 drug-like biaryl torsions, compared against high-fidelity reference energies. The values inside the parentheses were taken from Ref. [76].

Universal MLIP	MAE (kcal/mol)
MACE-OFF23-large	0.403 (0.3)
MACE-Osaka24-large	0.457
MACE-OFF23-small	0.598 (0.5)
MACE-Osaka24-small	0.695
GFN2-xTB	0.898
MACE-MP-0-large	1.909
SO3LR	2.451
MACE-MP-0-small	3.386

TABLE II. Mean absolute errors (MAEs) of reaction energy and energy barrier predictions of 10,073 reactions in Transition1x dataset. The units are all in eV.

Universal MLIPs	Reaction energy	Energy barrier
MACE-Osaka24-large	0.404	0.265
MACE-Osaka24-small	0.457	0.336
MACE-OFF23-large	0.711	0.436
MACE-OFF23-small	0.672	0.544
MACE-MP-0-large	0.937	0.519
MACE-MP-0-small	1.333	0.686

tion conditions for the crystal benchmarks can be found in Appendix VII C 5. The benchmark results for each crystal and crystal structure are discussed in detail in Appendix VII D. Fig. 3(b) shows the error distributions of lattice constant predictions calculated using various universal MLIPs and VASP at the same computational level as the training data, specifically the PBE functional. The MAEs of the MACE-Osaka24 models are larger than those of the MACE-MP-0 models. However, as shown in Table III, the MAEs of the predictions made by both the MACE-MP-0 and MACE-Osaka24 models are lower than those of the predictions made by the pretrained M3GNet model. The differences in predictive accuracy between MACE-MP-0 and MACE-Osaka24 were 0.008 Å and 0.002 Å for small and large models, respectively. This suggests that integrating data of organic molecules with different fidelities and domains using TEA does not deteriorate the original predictive accuracy. Fig. 3(c) shows the PES for the lattice constant of diamond Si as an example. All models accurately predict the equilibrium lattice constant at the PBE level calculated using VASP (calculation conditions of the MPStaticSet of the Materials Project). Furthermore, the performance of PES description was better in MACE-Osaka24 compared to MACE-MP-0 with respect to the VASP calculation results. This is likely coincidental but demonstrates the high robustness of multi-domain universal MLIPs.

Finally, Fig. 3(d) shows the radial distribution function (RDF) of O–O atoms obtained by MD of bulk liquid water at room temperature (300 K), which is important for both organic and inorganic materials. The MACE-MP-0 and MACE-Osaka24 models apply the D3(BJ) correction. Details of the MD calculations using MLIPs and classical force fields are pro-

TABLE III. Mean absolute errors (MAEs) of lattice constants predicted by universal machine learning interatomic potentials (MLIPs) compared to PBE-level DFT calculations for bulk crystals

Universal MLIP	MAE (Å)
MACE-MP-0-small	0.012
MACE-MP-0-large	0.016
MACE-Osaka24-large	0.018
MACE-Osaka24-small	0.020
M3GNet-MPF2021.2.8	0.021

vided in Appendix VII C 6. The MACE-OFF23 model describes the properties of liquid water at room temperature well. [76] MACE-MP-0-D3(BJ) reproduces the RDF at the PBE-D3(BJ) level. [59] Our MACE-Osaka24-large-D3(BJ) provides RDF descriptions almost equivalent to MACE-MP0-D3(BJ). On the other hand, MACE-Osaka24-small-D3(BJ) gives an RDF that is approximately intermediate between MACE-MP-0 and MACE-OFF23. This suggests that the ability to describe dynamic properties changes significantly depending on the complexity of the architecture and the balance of the dataset.

V. DISCUSSION

Our results show that TEA is an effective way to combine different datasets. By aligning inner-core reference energies and adjusting atomization energies, TEA bridges differences caused by varying computational details such as basis sets and exchange-correlation functionals. Using TEA, we merged the MPtrj inorganic crystal dataset with the OFF23 organic dataset to train MACE-Osaka24—a multi-domain MLIP that achieves accuracy on par with specialized models like MACE-MP-0 and MACE-OFF23, while covering a much wider range of chemical systems.

The key advantage of TEA is that it simplifies data integration without changing the MLIP’s architecture. Unlike methods such as Δ -machine learning or multi-fidelity SevenNet, which often target specific domains or fidelity levels, TEA offers a general, straightforward way to combine datasets. This approach allows researchers to use existing data from various sources without extensive recalculations. By showing that a single model—MACE-Osaka24—can accurately predict molecular reaction energies, lattice constants in inorganic crystals, and the properties of liquid water, we confirm that the resulting PES maintains physical consistency and meaningful energy gradients across diverse chemical environments.

Nonetheless, some limitations and challenges remain. The current implementation relies on the availability of suitable reference atomic energies and reference geometries, which can be more difficult for systems with strong electron correlations, charged species, or relativistic effects. While using a single global scaling factor for atomization energies worked well here, certain specialized cases may need more nuanced correction schemes. Future improvements might include adaptive correction functions or machine learning models that predict fidelity differences, further enhancing TEA’s generality and accuracy.

Future work could test TEA on datasets obtained from higher-level quantum chemical methods or directly include correlation and relativistic effects. Continued advances in neural network architectures, training methods, and hyperparameter optimization will also likely improve the robustness and accuracy of universal MLIPs. As re-

search communities produce larger and more varied first-principles datasets, the concepts demonstrated by TEA and MACE-Osaka24 can guide the development of more fully integrated and widely accessible foundation models. Such models, firmly based on reliable first-principles accuracy yet adaptable to different computational approaches, will help us better explore and understand increasingly complex chemical systems.

VI. CONCLUSION

We introduced the Total Energy Alignment (TEA) methodology as a robust and efficient framework for unifying heterogeneous quantum chemical datasets into a single-level potential energy surface. Using TEA, we created MACE-Osaka24, a single universal MLIP that achieves state-of-the-art accuracy for both molecular and crystalline systems. It matches the performance of specialized models like MACE-MP-0 for inorganic solids and MACE-OFF23 for organic molecules, all without expensive recalculations under a single theoretical framework.

The impact of TEA goes beyond its technical contributions. By enabling the integration of diverse datasets without expensive recalculations, it helps democratize the development of foundation models in chemistry. This approach aligns with the move toward open science, where using a wide range of data sources is increasingly essential. As the chemistry and materials science communities continue to produce larger, more varied datasets, TEA provides a practical route to truly universal MLIPs, accelerating the discovery of materials, drugs, and catalysts through collaborative, data-driven research.

ACKNOWLEDGMENTS

This project was supported by funding from the MEXT Quantum Leap Flagship Program (MEXTQLEAP) through Grant No. JPMXS0120319794, the JST COI-NEXT Program through Grant No. JPMJPF2014, and the JST ASPIRE Program Grant No. JPMJAP2319. The completion of this research was partially facilitated by the JSPS Grants-in-Aid for Scientific Research (KAKENHI), specifically Grant Nos. JP23H03819 and JP21K18933. We thank the Supercomputer Center, the Institute for Solid State Physics, the University of Tokyo, for allowing us to use their facilities. A part of the calculations were performed using the Genkai supercomputer of the Research Institute for Information Technology at Kyushu University. This work was also achieved using the SQUID supercomputer at the Cybermedia Center, Osaka University.

VII. APPENDIX

A. Total Energy Alignment for QM9 Dataset

1. Verification of TEA method

To evaluate the performance of the TEA method between datasets that, despite employing the same fidelity functionals, differ in core electron treatments, basis sets, and periodic boundary conditions, we conducted TEA between the quantum chemistry software packages VASP[79–82] and Amsterdam Density Functional (ADF) [84]. We utilized the QM9 dataset, which comprises approximately 134,000 molecules optimized at the B3LYP/6-31G(d) level using Gaussian09.[43] By performing single-point energy calculations at the PBE/PW level with VASP on the Gaussian09-optimized geometries, we generated a new dataset referred to as QM9VASP. For the TEA target, we adopted the PBE/TZP level dataset from MultiXC-QM9[44]—calculated using ADF with various functionals—which excludes molecules involving charge separation[112]; we will hereafter refer to this dataset as QM9ADF.

First, we demonstrate the performance of TEA using the QM9 dataset, a representative dataset of stable geometries of organic molecules. Fig. 4(a) shows the parity plot of atomization energies between QM9VASP and QM9ADF. Although QM9VASP and QM9ADF are calculated using the same functional, systematic differences with an RMSE of 0.3258 eV are observed. As shown in Fig. 4(b), by performing TEA using ICEA, the total energies of both agree with an RMSE of 0.3258 eV. This indicates that TEA is feasible without correction for functionals calculated at the same level. Furthermore, by performing TEA (ICEA/AEC), the RMSE of the total energies between the two improves to 0.0992 eV.

Similarly, Fig. 4(c) shows the parity plot comparing QM9VASP and QM9Psi4. There is no clear trend in the total energies between the two datasets, and the data points are scattered. This is because QM9Psi4 is calculated using an all-electron method, and the total energy is the energy of all electrons, while QM9VASP, as mentioned earlier, is the total energy of valence electrons only. As shown in Fig. 4(d), by performing TEA using ICEA, we succeeded in aligning the total energies to be comparable. However, the accuracy is as large as 4.2017 eV, and the reliability is low. This is mainly due to differences in fidelity caused by different functionals. TEA using ICEA/AEC captures systematic differences arising from fidelity variations and significantly improves the RMSE to 0.8388 eV.

B. Training Multi-domain Universal MLIPs

We demonstrate that stable training of universal MLIPs is possible by integrating datasets of the organic domain, to which TEA has been applied, into datasets of the inorganic domain. In this paper, as shown in Fig. 5(a), we constructed a TEA-MPTrj/OFF23 dataset by integrating the TEA-OFF23 dataset, which uses the scaling factor of AEC to QM9, into MPTrj of the Materials Project. For the MLIP architecture, we adopted the MACE small and large architectures proposed by Batatia et al.[59]. The constructed multi-domain universal MLIPs are referred to as MACE-Osaka24-small and MACE-Osaka24-large, respectively. Fig. 5(b)–(d) shows the learning curves of the MACE-Osaka24 models for energy, force, and stress. It was confirmed that the RMSEs tend to be smaller for the large model with a larger model size compared to the small model. This is in good agreement with the trend of learning curves shown in the paper by Batatia et al.[59].

C. Computational Details

1. QM9VASP Dataset Generation

QM9VASP dataset was generated using the Vienna Ab initio Simulation Package (VASP) version 5.4.4. For the exchange-correlation functional, we adopted the PBE functional used in generating MPTrj dataset. A plane-wave energy cutoff of 400 eV was employed for the expansion of the electronic wave functions (ENCUT = 400). The geometries were taken from the original QM9 dataset. To prevent interactions between adjacent unit cells, a vacuum layer of 10 Å was introduced in each unit cell. The electronic self-consistency loop was considered converged when the total energy change between successive iterations was less than 1×10^{-5} eV (EDIFF = 1e-05). Symmetry operations were disabled (ISYM = 0). High-precision settings were applied throughout the calculations (PREC = Accurate) to ensure reliable results. The Brillouin zone integrations were performed using the Gaussian smearing method with a smearing width of 0.1 eV (ISMEAR = 0, SIGMA = 0.1).

2. QM9Psi4 Dataset Generation

The QM9Psi4 dataset was generated using Psi4 version 1.9. To ensure that the computational conditions are equivalent to those employed in generating the OFF23 dataset, we adopted the ω B97M-D3(BJ) functional, which adds the D3 dispersion correction with the Becke-Johnson (BJ) damping function to the exchange-correlation functional ω B97M. The def2-TZVPPD basis set was used in all calculations.

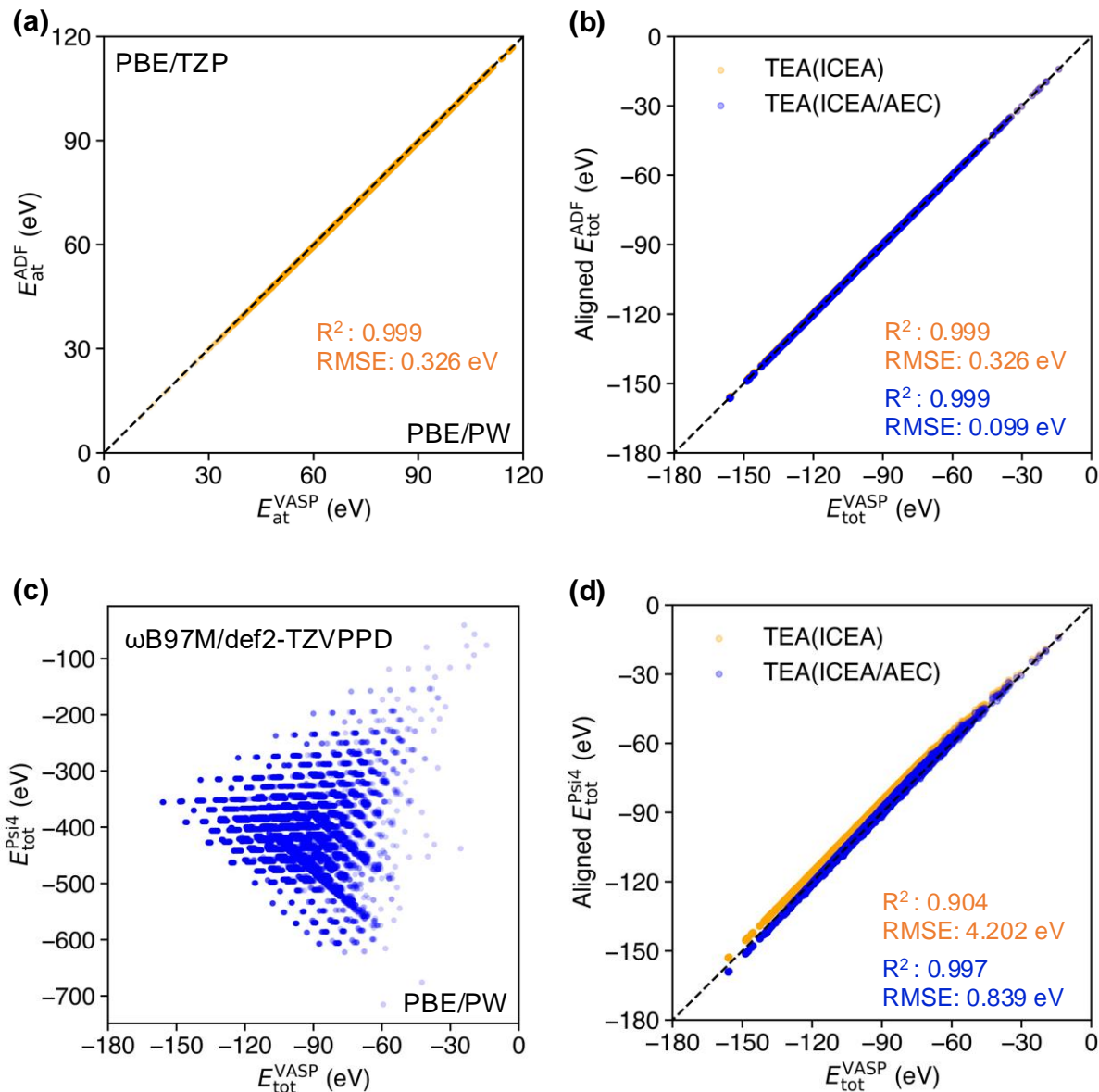


FIG. 4. The total energy alignment (TEA) results for different datasets. (a) Parity plot of atomization energies between QM9VASP and QM9ADF datasets using the same PBE functional. (b) Parity plot of the total energies after applying Inner Core Energy Alignment (ICEA) and Atomization Energy Correction (AEC) to the QM9ADF dataset. (c) Parity plot of total energies between QM9VASP and QM9Psi4 datasets before alignment, illustrating significant discrepancies due to differences in computational methods. (d) Parity plot after applying TEA (ICEA/AEC) to the QM9Psi4 dataset.

3. Biaryl Torsion Benchmark

First, we introduce the method for generating the biaryl torsion dataset by Lahey et al. [106], which provides the reference energies at the coupled cluster level as shown in Table I. The torsional PES were computed using density-fitting Møller-Plesset perturbation theory at second order (DF-MP2) with the def2-TZVP basis set (DF-MP2/def2-TZVP). CCSD(T1)* / CBS energies were

obtained by combining DLPNO-CCSD(T) (denoted as CCSD(T)*)[130], the complete basis set (CBS) correction scheme proposed by Smith et al.[70, 106], and iterative triples CCSD(T1) methods [130]. These torsional PES values serve as the reference data for present study.

We performed torsional PES optimizations using GFN2-xTB [107], MACE-MP-0, SO3LR [75], MACE-OFF23, MACE-Osaka24, VASP, and Psi4 on the dihedral torsions of 78 molecules presented in the biaryl torsion

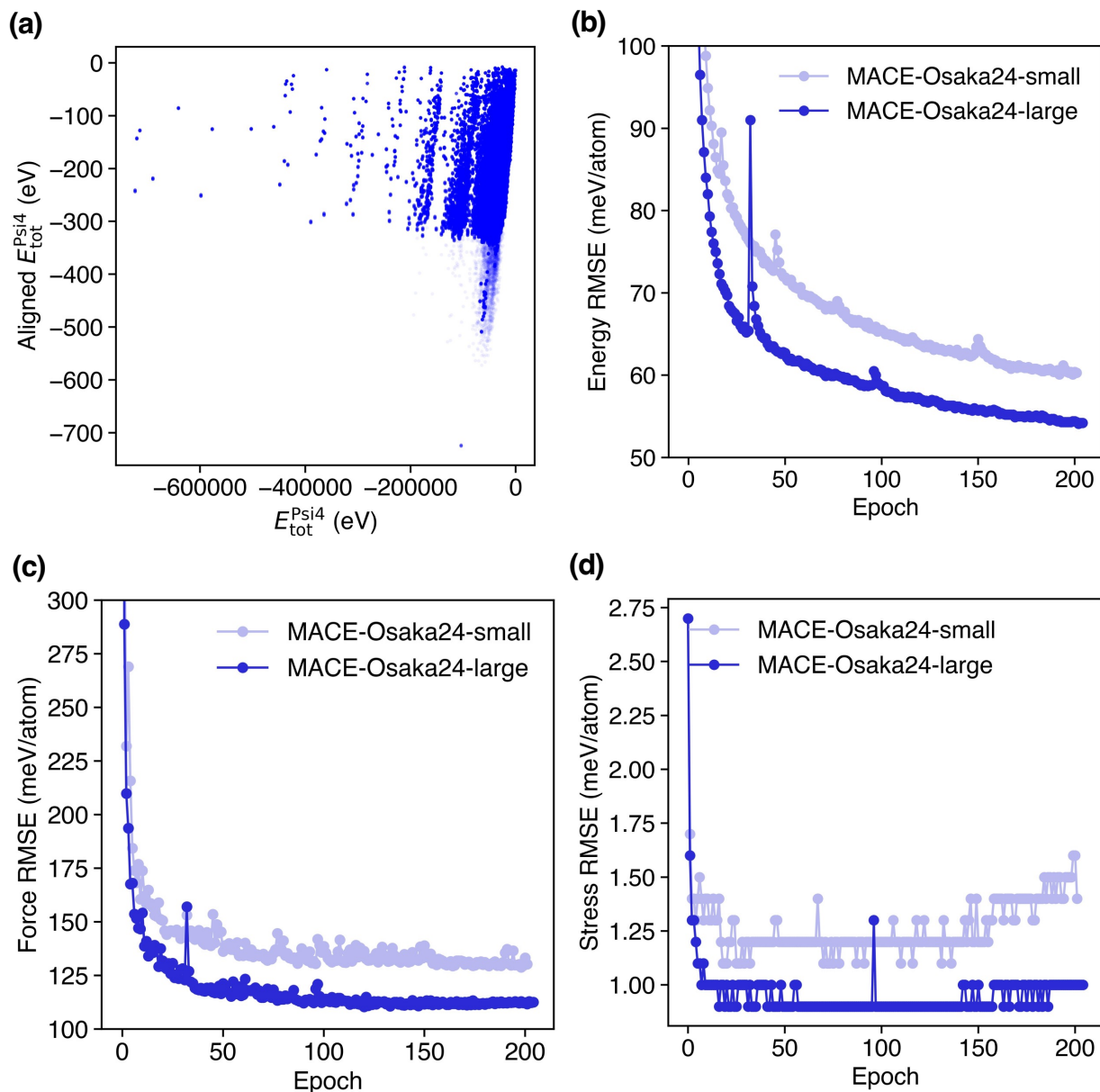


FIG. 5. (a) Parity plot of total energies from the original OFF23 dataset and after application of total energy alignment (TEA). (b) Energy root mean square error (RMSE) during training of MACE-Osaka24-small and MACE-Osaka24-large models over 200 epochs. (c) Force RMSE during training of the same models. (d) Stress RMSE during training of the same models.

benchmark [106]. In calculations with GFN2-xTB and all MLIPs, the dihedral angles were varied in 5° increments, and structure relaxations were performed under the constraint that each dihedral angle remained fixed at its set value. For VASP and Psi4, the dihedral angle increments were set to 10° . In all methods, geometry relaxations were carried out until the force acting on each atom was less than 0.01 eV/\AA . All constrained geometry optimization calculations were implemented using Atomic Simulation Environment (ASE) version 3.23.0. [118] It should be noted that in the work by Kovács et al. [76], the tor-

sional PES optimization was performed using Torsion-Drive [117] algorithm.

4. Benchmark on Transition1x

The original Transition1x dataset was generated using ORCA version 5.0.2 with the exchange functional ωB97x and the basis set 6-31G(d). Since our constructed MACE-Osaka24 models are based on the OFF23 dataset computed with Psi4, we performed single-point calcula-

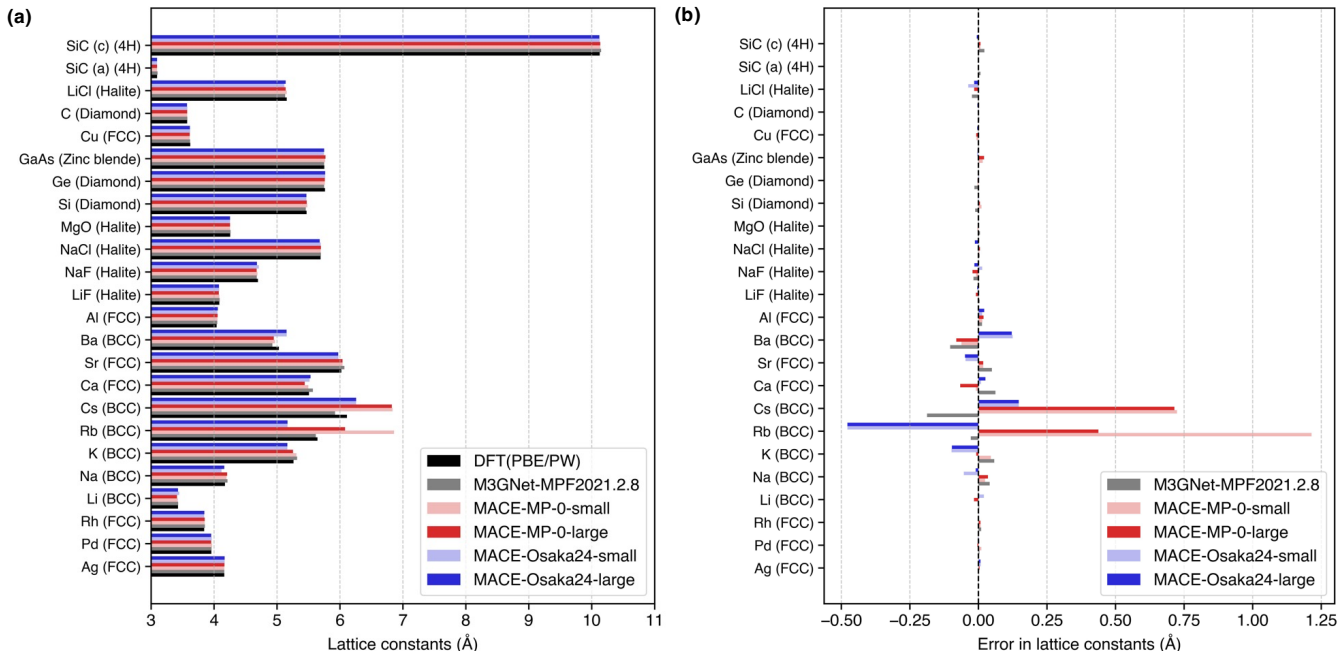


FIG. 6. (a) Lattice constants of bulk crystals predicted by universal MLIPs and by DFT calculations using the PBE functional with VASP, which is at the same theoretical level as the training data of the universal MLIPs presented in the Results section. (b) Prediction errors of the universal MLIPs relative to the lattice constants predicted by DFT.

tions on the initial state, transition state, and final state geometries of the 10,073 reactions provided in Transition1x dataset using Psi4 under the computational conditions specified in Appendix VII C 2 to ensure compatibility. Similarly, all validations using MLIPs and GFN2-xTB were carried out by performing single-point calculations on the IS, TS, and FS geometries provided in Transition1x.

5. Bulk Crystal Lattice Constant

The crystals used for the benchmark were those adopted in Section B.4 of the Supporting Information in the paper by Batatia et al [23]. For the BCC materials K, Rb, and Cs, it was not possible to represent them using the 4.5 Å cutoff radius employed in the graph construction for the MACE-Osaka24 models, and therefore they were excluded for benchmark in Section IV. Further details can be found in Appendix VII D. The optimization of lattice constants through first-principles calculations was performed using VASP at PBE level. To ensure compatibility with the MPtrj dataset used for training the MACE-MP-0 and MACE-Osaka24 models, input parameters from the MPRelaxSet in the pymatgen [116] library of the Materials Project were utilized. For the MACE-MP-0 and MACE-Osaka24 models, the convergence criterion for unit cell optimization was set to 0.01 eV/Å. First-principle PES calculations for Si as a function of lattice constants, shown in Fig. 3(c), were per-

formed using single-point calculations with inputs from the MPStaticSet in pymatgen. The lattice constants were varied from 5 Å to 6 Å in increments of 0.01 Å.

6. Molecular Dynamics of Liquid Water

Classical MD simulations were performed using GRO-MACS version 2023.3. [120] The TIP3P [121] and TIP4P/2005 [122] water models were employed as the force fields. The TIP4P/2005 model was chosen as a reference for evaluating the accuracy of MLIPs because it reproduces the thermodynamic properties of water with high accuracy over a wide temperature range [123]. For ML-driven MD simulations, the interface with MACE was implemented using a modified version of OpenMM-ML [119], enabling the incorporation of D3(BJ) dispersion force corrections. Simulations were conducted in a PBC box containing 64 H₂O molecules with a density of 1 g/cm³. For ML-driven MD, NVT ensemble simulations were performed for 100 ps, with the final 50 ps used for analysis. For classical MD, simulations were carried out in an NVT ensemble with 1,000 H₂O molecules for 1,000 ps, with the last 500 ps utilized for analysis.

D. Material-wise Lattice Constants

In this section, we discuss the results of lattice constant predictions for representative bulk crystals presented in

TABLE IV. Table III. Mean absolute errors (MAEs) of lattice constants (in Å) predicted by universal MLIPs compared to DFT with PBE using VASP, categorized by crystal structure type. The predictions from M3GNet-MPF2021.2.8, MACE-MP-0-small, MACE-MP-0-large, MACE-Osaka24-small, and MACE-Osaka24-large models are evaluated across various structures including 4H, BCC, Diamond, FCC, Halite, and Zinc blende. The errors correspond to the deviations shown in Fig. 6(b).

Crystal structure	M3GNet-MPF2021.2.8	MACE-MP-0-small	MACE-MP-0-large	MACE-Osaka24-small	MACE-Osaka24-large
4H	0.0143	0.0036	0.0042	0.0002	0.0033
BCC	0.0701	0.3453	0.2153	0.1536	0.1423
Diamond	0.0100	0.0047	0.0031	0.0020	0.0029
FCC	0.0200	0.0096	0.0179	0.0118	0.0156
Halite	0.0111	0.0036	0.0108	0.0113	0.0100
Zinc blende	0.0017	0.0153	0.0205	0.0049	0.0031

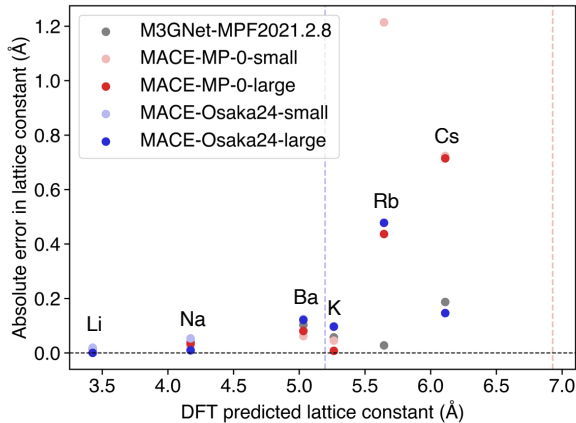


FIG. 7. Absolute errors in lattice constant predictions as a function of DFT-predicted lattice constants for body centered cubic (BCC)-type crystals using various universal MLIPs. The models compared are M3GNet-MPF2021.2.8, MACE-MP-0 (small and large), and MACE-Osaka24 (small and large). The graph construction cutoff radii for the MACE-MP-0 and M3GNet models are 6.0 Å, with the range of lattice constants these models can consider indicated by the red dashed line. For the MACE-Osaka24 model, the cutoff radius is 4.5 Å, and the corresponding range of lattice constants is shown by the blue dashed line. Specific elements (Li, Na, K, Rb, Cs, Ba) are labeled for clarity.

the Results section, as well as the predictive performance for each crystal structure. Fig. 6 shows the predicted lattice constants obtained from DFT and universal MLIPs.

As shown in Fig. 6(b), the predictions by M3GNet-MPF2021.2.8 exhibit the fewest outliers among the models. As indicated in Table III, the M3GNet-MPF2021.2.8, MACE-MP-0, and MACE-Osaka24 MLIPs achieve prediction accuracies with mean absolute errors (MAEs) below 0.02 Å for crystal structures other than body-centered cubic (BCC). However, in predicting BCC-type crystal structures, they exhibit larger prediction errors compared to other crystal structures. The poor predictive performance for BCC crystals may be related to the cutoff radius used in graph construction. Fig. 7 shows the DFT-predicted lattice constants of BCC crystals and the absolute errors of the lattice constant predictions. As the lattice constant increases, the prediction errors of all models also increase. MACE-Osaka24 is constructed with a cutoff radius of 4.5 Å, while M3GNet-MPF2021.2.8 and MACE-MP-0 are constructed with a cutoff radius of 6.0 Å. Therefore, the maximum lattice constants of BCC crystals that each model can capture are 5.196 Å for MACE-Osaka24 and 6.928 Å for M3GNet-MPF2021.2.8 and MACE-MP-0. Predictions for larger lattice constants result in a superposition of isolated atoms and simple cubic lattice crystals, failing to properly capture the BCC crystal structure. Thus, MACE-Osaka24 cannot be applied to predict the lattice constants of K, Rb, and Cs. On the other hand, although M3GNet and MACE-MP-0 have cutoff radii exceeding the lattice constants of the target BCC crystals, their predictions tend to approach lattice constants near the cutoff radius, suggesting that using larger cutoff radii may be necessary for improvement.

- [1] G. Wang, C. Wang, X. Zhang, Z. Li, J. Zhou, and Z. Sun, Machine learning interatomic potential: Bridge the gap between small-scale models and realistic device-scale simulations, *Iscience* **27** (2024).
- [2] S. Käser, L. I. Vazquez-Salazar, M. Meuwly, and K. Töpfer, Neural network potentials for chemistry: concepts, applications and prospects, *Digital Discovery* **2**, 28 (2023).
- [3] K. Choudhary, B. DeCost, C. Chen, A. Jain, F. Tavazza, R. Cohn, C. W. Park, A. Choudhary, A. Agrawal, S. J. Billinge, *et al.*, Recent advances and applications of deep learning methods in materials science, *npj Computational Materials* **8**, 59 (2022).
- [4] J. Schmidt, M. R. Marques, S. Botti, and M. A. Marques, Recent advances and applications of machine learning in solid-state materials science, *npj computational materials* **5**, 83 (2019).

- [5] Y. Mishin, Machine-learning interatomic potentials for materials science, *Acta Materialia* **214**, 116980 (2021).
- [6] O. T. Unke, S. Chmiela, H. E. Sauceda, M. Gastegger, I. Poltavsky, K. T. Schütt, A. Tkatchenko, and K.-R. Müller, Machine learning force fields, *Chemical Reviews* **121**, 10142 (2021).
- [7] E. Kocer, T. W. Ko, and J. Behler, Neural network potentials: A concise overview of methods, *Annual review of physical chemistry* **73**, 163 (2022).
- [8] V. L. Deringer, M. A. Caro, and G. Csányi, Machine learning interatomic potentials as emerging tools for materials science, *Advanced Materials* **31**, 1902765 (2019).
- [9] S. Chmiela, V. Vassilev-Galindo, O. T. Unke, A. Kabylda, H. E. Sauceda, A. Tkatchenko, and K.-R. Müller, Accurate global machine learning force fields for molecules with hundreds of atoms, *Science Advances* **9**, eadf0873 (2023).
- [10] T. Mueller, A. Hernandez, and C. Wang, Machine learning for interatomic potential models, *The Journal of chemical physics* **152** (2020).
- [11] P. Liu, J. Wang, N. Avargues, C. Verdi, A. Singraber, F. Karsai, X.-Q. Chen, and G. Kresse, Combining machine learning and many-body calculations: coverage-dependent adsorption of co on rh (111), *Physical Review Letters* **130**, 078001 (2023).
- [12] A. P. Bartók, M. C. Payne, R. Kondor, and G. Csányi, Gaussian approximation potentials: The accuracy of quantum mechanics, without the electrons, *Physical review letters* **104**, 136403 (2010).
- [13] J. Behler and M. Parrinello, Generalized neural-network representation of high-dimensional potential-energy surfaces, *Physical review letters* **98**, 146401 (2007).
- [14] J. Behler, Atom-centered symmetry functions for constructing high-dimensional neural network potentials, *The Journal of chemical physics* **134** (2011).
- [15] K. T. Schütt, H. E. Sauceda, P.-J. Kindermans, A. Tkatchenko, and K.-R. Müller, SchNet—a deep learning architecture for molecules and materials, *The Journal of Chemical Physics* **148** (2018).
- [16] T. Xie and J. C. Grossman, Crystal graph convolutional neural networks for an accurate and interpretable prediction of material properties, *Physical review letters* **120**, 145301 (2018).
- [17] C. Chen, W. Ye, Y. Zuo, C. Zheng, and S. P. Ong, Graph networks as a universal machine learning framework for molecules and crystals, *Chemistry of Materials* **31**, 3564 (2019).
- [18] J. Gastegger, F. Becker, and S. Günnemann, Gemnet: Universal directional graph neural networks for molecules, *Advances in Neural Information Processing Systems* **34**, 6790 (2021).
- [19] O. T. Unke, S. Chmiela, M. Gastegger, K. T. Schütt, H. E. Sauceda, and K.-R. Müller, Spookynet: Learning force fields with electronic degrees of freedom and non-local effects, *Nature communications* **12**, 7273 (2021).
- [20] K. Choudhary and B. DeCost, Atomistic line graph neural network for improved materials property predictions, *npj Computational Materials* **7**, 185 (2021).
- [21] S. Takamoto, S. Izumi, and J. Li, Teanet: Universal neural network interatomic potential inspired by iterative electronic relaxations, *Computational Materials Science* **207**, 111280 (2022).
- [22] S. Batzner, A. Musaelian, L. Sun, M. Geiger, J. P. Mailoa, M. Kornbluth, N. Molinari, T. E. Smidt, and B. Kozinsky, E (3)-equivariant graph neural networks for data-efficient and accurate interatomic potentials, *Nature communications* **13**, 2453 (2022).
- [23] I. Batatia, D. P. Kovacs, G. Simm, C. Ortner, and G. Csányi, Mace: Higher order equivariant message passing neural networks for fast and accurate force fields, *Advances in Neural Information Processing Systems* **35**, 11423 (2022).
- [24] A. Musaelian, S. Batzner, A. Johansson, L. Sun, C. J. Owen, M. Kornbluth, and B. Kozinsky, Learning local equivariant representations for large-scale atomistic dynamics, *Nature Communications* **14**, 579 (2023).
- [25] Z. Mao, J. Li, C. Liang, D. Das, M. Sumita, and K. Tsuda, Molecule graph networks with many-body equivariant interactions (2024), arXiv:2406.13265 [cs.LG].
- [26] J. T. Frank, O. T. Unke, K.-R. Müller, and S. Chmiela, A euclidean transformer for fast and stable machine learned force fields, *Nature Communications* **15**, 6539 (2024).
- [27] Y. Park, J. Kim, S. Hwang, and S. Han, Scalable parallel algorithm for graph neural network interatomic potentials in molecular dynamics simulations, *Journal of Chemical Theory and Computation* (2024).
- [28] B. Cheng, Cartesian atomic cluster expansion for machine learning interatomic potentials, *npj Computational Materials* **10**, 157 (2024).
- [29] J. Wang, Y. Wang, H. Zhang, Z. Yang, Z. Liang, J. Shi, H.-T. Wang, D. Xing, and J. Sun, E (n)-equivariant cartesian tensor message passing interatomic potential, *Nature Communications* **15**, 7607 (2024).
- [30] A. Duval, S. V. Mathis, C. K. Joshi, V. Schmidt, S. Miret, F. D. Malliaros, T. Cohen, P. Lio, Y. Bengio, and M. Bronstein, A hitchhiker’s guide to geometric gns for 3d atomic systems, arXiv preprint arXiv:2312.07511 (2023).
- [31] A. Jain, S. P. Ong, G. Hautier, W. Chen, W. D. Richards, S. Dacek, S. Cholia, D. Gunter, D. Skinner, G. Ceder, *et al.*, Commentary: The materials project: A materials genome approach to accelerating materials innovation, *APL materials* **1** (2013).
- [32] S. Kirklin, J. E. Saal, B. Meredig, A. Thompson, J. W. Doak, M. Aykol, S. Rühl, and C. Wolverton, The open quantum materials database (oqmd): assessing the accuracy of dft formation energies, *npj Computational Materials* **1**, 1 (2015).
- [33] J. Schmidt, H.-C. Wang, T. F. Cerqueira, S. Botti, and M. A. Marques, A dataset of 175k stable and metastable materials calculated with the pbesol and scan functionals, *Scientific Data* **9**, 64 (2022).
- [34] J. Schmidt, T. F. Cerqueira, A. H. Romero, A. Loew, F. Jäger, H.-C. Wang, S. Botti, and M. A. Marques, Improving machine-learning models in materials science through large datasets, *Materials Today Physics* , 101560 (2024).
- [35] S. Haastrup, M. Strange, M. Pandey, T. Deilmann, P. S. Schmidt, N. F. Hinsche, M. N. Gjerding, D. Torelli, P. M. Larsen, A. C. Riis-Jensen, *et al.*, The computational 2d materials database: high-throughput modeling and discovery of atomically thin crystals, *2D Materials* **5**, 042002 (2018).

- [36] A. S. Rosen, S. M. Iyer, D. Ray, Z. Yao, A. Aspuru-Guzik, L. Gagliardi, J. M. Notestein, and R. Q. Snurr, Machine learning the quantum-chemical properties of metal-organic frameworks for accelerated materials discovery, *Matter* **4**, 1578 (2021).
- [37] A. Sriram, S. Choi, X. Yu, L. M. Brabson, A. Das, Z. Ulissi, M. Uyttendaele, A. J. Medford, and D. S. Sholl, The open dac 2023 dataset and challenges for sorbent discovery in direct air capture (2024).
- [38] L. Chanussot, A. Das, S. Goyal, T. Lavril, M. Shuaibi, M. Riviere, K. Tran, J. Heras-Domingo, C. Ho, W. Hu, *et al.*, Open catalyst 2020 (oc20) dataset and community challenges, *Acs Catalysis* **11**, 6059 (2021).
- [39] R. Tran, J. Lan, M. Shuaibi, B. M. Wood, S. Goyal, A. Das, J. Heras-Domingo, A. Kolluru, A. Rizvi, N. Shoghi, *et al.*, The open catalyst 2022 (oc22) dataset and challenges for oxide electrocatalysts, *ACS Catalysis* **13**, 3066 (2023).
- [40] J. S. Smith, O. Isayev, and A. E. Roitberg, Ani-1, a data set of 20 million calculated off-equilibrium conformations for organic molecules, *Scientific data* **4**, 1 (2017).
- [41] J. S. Smith, R. Zubatyuk, B. Nebgen, N. Lubbers, K. Barros, A. E. Roitberg, O. Isayev, and S. Tretiak, The ani-1ccx and ani-1x data sets, coupled-cluster and density functional theory properties for molecules, *Scientific data* **7**, 134 (2020).
- [42] M. Schreiner, A. Bhowmik, T. Vegge, J. Busk, and O. Winther, Transition1x-a dataset for building generalizable reactive machine learning potentials, *Scientific Data* **9**, 779 (2022).
- [43] R. Ramakrishnan, P. O. Dral, M. Rupp, and O. A. Von Lilienfeld, Quantum chemistry structures and properties of 134 kilo molecules, *Scientific data* **1**, 1 (2014).
- [44] S. Nandi, T. Vegge, and A. Bhowmik, Multixc-qm9: Large dataset of molecular and reaction energies from multi-level quantum chemical methods, *Scientific data* **10**, 783 (2023).
- [45] M. Nakata and T. Shimazaki, Pubchemqc project: a large-scale first-principles electronic structure database for data-driven chemistry, *Journal of chemical information and modeling* **57**, 1300 (2017).
- [46] M. Nakata and T. Maeda, Pubchemqc b3lyp/6-31g*//pm6 data set: The electronic structures of 86 million molecules using b3lyp/6-31g* calculations, *Journal of Chemical Information and Modeling* **63**, 5734 (2023).
- [47] P. Eastman, P. K. Behara, D. L. Dotson, R. Galvelis, J. E. Herr, J. T. Horton, Y. Mao, J. D. Chodera, B. P. Pritchard, Y. Wang, *et al.*, Spice, a dataset of drug-like molecules and peptides for training machine learning potentials, *Scientific Data* **10**, 11 (2023).
- [48] C. Isert, K. Atz, J. Jiménez-Luna, and G. Schneider, Qmugs, quantum mechanical properties of drug-like molecules, *Scientific Data* **9**, 273 (2022).
- [49] A. G. Donchev, A. G. Taube, E. Decolvenaere, C. Hargus, R. T. McGibbon, K.-H. Law, B. A. Gregersen, J.-L. Li, K. Palmo, K. Siva, *et al.*, Quantum chemical benchmark databases of gold-standard dimer interaction energies, *Scientific data* **8**, 55 (2021).
- [50] T. Zhou, Z. Song, and K. Sundmacher, Big data creates new opportunities for materials research: a review on methods and applications of machine learning for materials design, *Engineering* **5**, 1017 (2019).
- [51] A. Ullah, Y. Chen, and P. O. Dral, Molecular quantum chemical data sets and databases for machine learning potentials (2024), arXiv:2408.12058 [physics.chem-ph].
- [52] C. Gabellini, N. Shenoy, S. Thaler, S. Canturk, D. McNeela, D. Beaini, M. Bronstein, and P. Tossou, Openqdc: Open quantum data commons, arXiv preprint arXiv:2411.19629 (2024).
- [53] A. Bochkarev, Y. Lysogorskiy, and R. Drautz, Graph atomic cluster expansion for semilocal interactions beyond equivariant message passing, *Physical Review X* **14**, 021036 (2024).
- [54] C. Chen and S. P. Ong, A universal graph deep learning interatomic potential for the periodic table, *Nature Computational Science* **2**, 718 (2022).
- [55] J. Qi, T. W. Ko, B. C. Wood, T. A. Pham, and S. P. Ong, Robust training of machine learning interatomic potentials with dimensionality reduction and stratified sampling, *npj Computational Materials* **10**, 43 (2024).
- [56] S. Takamoto, C. Shinagawa, D. Motoki, K. Nakago, W. Li, I. Kurata, T. Watanabe, Y. Yayama, H. Iriguchi, Y. Asano, *et al.*, Towards universal neural network potential for material discovery applicable to arbitrary combination of 45 elements, *Nature Communications* **13**, 2991 (2022).
- [57] B. Deng, P. Zhong, K. Jun, J. Riebesell, K. Han, C. J. Bartel, and G. Ceder, Chgnet as a pretrained universal neural network potential for charge-informed atomistic modelling, *Nature Machine Intelligence* **5**, 1031 (2023).
- [58] K. Choudhary, B. DeCost, L. Major, K. Butler, J. Thiyagalingam, and F. Tavazza, Unified graph neural network force-field for the periodic table: solid state applications, *Digital Discovery* **2**, 346 (2023).
- [59] I. Batatia, P. Benner, Y. Chiang, A. M. Elena, D. P. Kovács, J. Riebesell, X. R. Advincula, M. Asta, M. Avaylon, W. J. Baldwin, F. Berger, N. Bernstein, A. Bhowmik, S. M. Blau, V. Cărare, J. P. Darby, S. De, F. D. Pia, V. L. Deringer, R. Elijošius, Z. El-Machachi, F. Falcioni, E. Fako, A. C. Ferrari, A. Genreith-Schriever, J. George, R. E. A. Goodall, C. P. Grey, P. Grigorev, S. Han, W. Handley, H. H. Heenen, K. Hermansson, C. Holm, J. Jaafar, S. Hofmann, K. S. Jakob, H. Jung, V. Kapil, A. D. Kaplan, N. Karimitari, J. R. Kermode, N. Kroupa, J. Kullgren, M. C. Kuner, D. Kuryla, G. Liepuoniute, J. T. Margraf, I.-B. Magdău, A. Michaelides, J. H. Moore, A. A. Naik, S. P. Niblett, S. W. Norwood, N. O'Neill, C. Ortner, K. A. Persson, K. Reuter, A. S. Rosen, L. L. Schaaf, C. Schran, B. X. Shi, E. Sivonxay, T. K. Stenczel, V. Svahn, C. Sutton, T. D. Swinburne, J. Tilly, C. van der Oord, E. Varga-Umbrich, T. Vegge, M. Vondrák, Y. Wang, W. C. Witt, F. Zills, and G. Csányi, A foundation model for atomistic materials chemistry (2024), arXiv:2401.00096 [physics.chem-ph].
- [60] A. Merchant, S. Batzner, S. S. Schoenholz, M. Aykol, G. Cheon, and E. D. Cubuk, Scaling deep learning for materials discovery, *Nature* **624**, 80 (2023).
- [61] H. Yang, C. Hu, Y. Zhou, X. Liu, Y. Shi, J. Li, G. Li, Z. Chen, S. Chen, C. Zeni, M. Horton, R. Pinsler, A. Fowler, D. Zügner, T. Xie, J. Smith, L. Sun, Q. Wang, L. Kong, C. Liu, H. Hao, and Z. Lu, MatterSim: A deep learning atomistic model across elements, temperatures and pressures (2024), arXiv:2405.04967 [cond-mat.mtrl-sci].

- [62] L. Barroso-Luque, M. Shuaibi, X. Fu, B. M. Wood, M. Dzamba, M. Gao, A. Rizvi, C. L. Zitnick, and Z. W. Ulissi, Open materials 2024 (omat24) inorganic materials dataset and models, arXiv preprint arXiv:2410.12771 (2024).
- [63] T. Shiota, K. Ishihara, and W. Mizukami, Universal neural network potentials as descriptors: towards scalable chemical property prediction using quantum and classical computers, *Digital Discovery* **3**, 1714 (2024).
- [64] T. Shiota, K. Ishihara, and W. Mizukami, Lowering the exponential wall: Accelerating high-entropy alloy catalysts screening using local surface energy descriptors from neural network potentials (2024), arXiv:2404.08413 [quant-ph].
- [65] M. Neumann, J. Gin, B. Rhodes, S. Bennett, Z. Li, H. Choubisa, A. Hussey, and J. Godwin, Orb: A fast, scalable neural network potential (2024), arXiv:2410.22570 [cond-mat.mtrl-sci].
- [66] B. Focassio, L. P. M. Freitas, and G. R. Schleder, Performance assessment of universal machine learning interatomic potentials: Challenges and directions for materials’ surfaces, *ACS Applied Materials & Interfaces* (2024).
- [67] H. Yu, M. Giantomassi, G. Materzanini, J. Wang, and G.-M. Rignanese, Systematic assessment of various universal machine-learning interatomic potentials, *Materials Genome Engineering Advances* **2**, e58 (2024).
- [68] J. S. Smith, O. Isayev, and A. E. Roitberg, Ani-1: an extensible neural network potential with dft accuracy at force field computational cost, *Chemical science* **8**, 3192 (2017).
- [69] J. S. Smith, B. Nebgen, N. Lubbers, O. Isayev, and A. E. Roitberg, Less is more: Sampling chemical space with active learning, *The Journal of chemical physics* **148** (2018).
- [70] J. S. Smith, B. T. Nebgen, R. Zubatyuk, N. Lubbers, C. Devereux, K. Barros, S. Tretiak, O. Isayev, and A. E. Roitberg, Approaching coupled cluster accuracy with a general-purpose neural network potential through transfer learning, *Nature communications* **10**, 2903 (2019).
- [71] C. Devereux, J. S. Smith, K. K. Huddleston, K. Barros, R. Zubatyuk, O. Isayev, and A. E. Roitberg, Extending the applicability of the ani deep learning molecular potential to sulfur and halogens, *Journal of Chemical Theory and Computation* **16**, 4192 (2020).
- [72] R. Zubatyuk, J. S. Smith, J. Leszczynski, and O. Isayev, Accurate and transferable multitask prediction of chemical properties with an atoms-in-molecules neural network, *Science advances* **5**, eaav6490 (2019).
- [73] D. Anstine, R. Zubatyuk, and O. Isayev, Aignet2: a neural network potential to meet your neutral, charged, organic, and elemental-organic needs, ChemRxiv preprint 10.26434/chemrxiv-2023-296ch-v2 (2024).
- [74] O. T. Unke, M. Stöhr, S. Ganscha, T. Unterthiner, H. Maennel, S. Kashubin, D. Ahlin, M. Gastegger, L. Medrano Sandonas, J. T. Berryman, *et al.*, Biomolecular dynamics with machine-learned quantum-mechanical force fields trained on diverse chemical fragments, *Science Advances* **10**, eadn4397 (2024).
- [75] A. Kabylda, J. T. Frank, S. S. Dou, A. Khabibrakhmanov, L. M. Sandonas, O. T. Unke, S. Chmiela, K.-R. Müller, and A. Tkatchenko, Molecular simulations with a pretrained neural network and universal pairwise force fields, ChemRxiv preprint 10.26434/chemrxiv-2024-bdfr0 (2024).
- [76] D. P. Kovács, J. H. Moore, N. J. Browning, I. Batafia, J. T. Horton, V. Kapil, W. C. Witt, I.-B. Magdău, D. J. Cole, and G. Csányi, Mace-off23: Transferable machine learning force fields for organic molecules, arXiv preprint arXiv:2312.15211 (2023).
- [77] G. R. Schleder, A. C. Padilha, C. M. Acosta, M. Costa, and A. Fazzio, From dft to machine learning: recent approaches to materials science—a review, *Journal of Physics: Materials* **2**, 032001 (2019).
- [78] B. Huang, G. F. von Rudorff, and O. A. von Lilienfeld, The central role of density functional theory in the ai age, *Science* **381**, 170 (2023).
- [79] G. Kresse and J. Hafner, Ab initio molecular dynamics for liquid metals, *Physical review B* **47**, 558 (1993).
- [80] G. Kresse and J. Furthmüller, Efficient iterative schemes for ab initio total-energy calculations using a plane-wave basis set, *Physical review B* **54**, 11169 (1996).
- [81] G. Kresse and J. Hafner, Ab initio molecular-dynamics simulation of the liquid-metal–amorphous-semiconductor transition in germanium, *Physical Review B* **49**, 14251 (1994).
- [82] G. Kresse and J. Furthmüller, Efficiency of ab-initio total energy calculations for metals and semiconductors using a plane-wave basis set, *Computational materials science* **6**, 15 (1996).
- [83] J. Hutter, M. Iannuzzi, F. Schiffmann, and J. VandeVondele, cp2k: atomistic simulations of condensed matter systems, *Wiley Interdisciplinary Reviews: Computational Molecular Science* **4**, 15 (2014).
- [84] G. t. Te Velde, F. M. Bickelhaupt, E. J. Baerends, C. Fonseca Guerra, S. J. van Gisbergen, J. G. Snijders, and T. Ziegler, Chemistry with adf, *Journal of Computational Chemistry* **22**, 931 (2001).
- [85] D. G. Smith, L. A. Burns, A. C. Simmonett, R. M. Parrish, M. C. Schieber, R. Galvelis, P. Kraus, H. Kruse, R. Di Remigio, A. Alenaizan, *et al.*, Psi4 1.4: Open-source software for high-throughput quantum chemistry, *The Journal of chemical physics* **152** (2020).
- [86] F. Neese, Software update: the orca program system, version 5.0, *WIREs Comput. Molec. Sci.* **12**, e1606 (2022).
- [87] F. Neese, The orca program system, *WIREs Comput. Molec. Sci.* **2**, 73 (2012).
- [88] M. J. Frisch, G. W. Trucks, H. B. Schlegel, G. E. Scuseria, M. A. Robb, J. R. Cheeseman, G. Scalmani, V. Barone, G. A. Petersson, H. Nakatsuji, X. Li, M. Caricato, A. V. Marenich, J. Bloino, B. G. Janesko, R. Gomperts, B. Mennucci, H. P. Hratchian, J. V. Ortiz, A. F. Izmaylov, J. L. Sonnenberg, D. Williams-Young, F. Ding, F. Lipparini, F. Egidi, J. Goings, B. Peng, A. Petrone, T. Henderson, D. Ranasinghe, V. G. Zakrzewski, J. Gao, N. Rega, G. Zheng, W. Liang, M. Hada, M. Ehara, K. Toyota, R. Fukuda, J. Hasegawa, M. Ishida, T. Nakajima, Y. Honda, O. Kitao, H. Nakai, T. Vreven, K. Throssell, J. A. Montgomery, Jr., J. E. Peralta, F. Ogliaro, M. J. Bearpark, J. J. Heyd, E. N. Brothers, K. N. Kudin, V. N. Staroverov, T. A. Keith, R. Kobayashi, J. Normand, K. Raghavachari, A. P. Rendell, J. C. Burant, S. S. Iyengar, J. Tomasi, M. Cossi, J. M. Millam, M. Klene, C. Adamo, R. Cammi, J. W. Ochterski, R. L. Martin, K. Morokuma, O. Farkas, J. B. Foresman, and D. J.

- Fox, Gaussian~16 Revision C.01 (2016), gaussian Inc. Wallingford CT.
- [89] D. Zhang, X. Liu, X. Zhang, C. Zhang, C. Cai, H. Bi, Y. Du, X. Qin, A. Peng, J. Huang, B. Li, Y. Shan, J. Zeng, Y. Zhang, S. Liu, Y. Li, J. Chang, X. Wang, S. Zhou, J. Liu, X. Luo, Z. Wang, W. Jiang, J. Wu, Y. Yang, J. Yang, M. Yang, F.-Q. Gong, L. Zhang, M. Shi, F.-Z. Dai, D. M. York, S. Liu, T. Zhu, Z. Zhong, J. Lv, J. Cheng, W. Jia, M. Chen, G. Ke, W. E. L. Zhang, and H. Wang, Dpa-2: a large atomic model as a multi-task learner (2024), arXiv:2312.15492 [physics.chem-ph].
- [90] R. Ramakrishnan, P. O. Dral, M. Rupp, and O. A. Von Lilienfeld, Big data meets quantum chemistry approximations: the δ -machine learning approach, *Journal of chemical theory and computation* **11**, 2087 (2015).
- [91] C. Chen, Y. Zuo, W. Ye, X. Li, and S. P. Ong, Learning properties of ordered and disordered materials from multi-fidelity data, *Nature Computational Science* **1**, 46 (2021).
- [92] M. Liu, A. Gopakumar, V. I. Hegde, J. He, and C. Wolverton, High-throughput hybrid-functional dft calculations of bandgaps and formation energies and multifidelity learning with uncertainty quantification, *Physical Review Materials* **8**, 043803 (2024).
- [93] J. Kim, J. Kim, J. Kim, J. Lee, Y. Park, Y. Kang, and S. Han, Data-efficient multi-fidelity training for high-fidelity machine learning interatomic potentials (2024), arXiv:2409.07947 [cond-mat.mtrl-sci].
- [94] A. Jain, G. Hautier, S. P. Ong, C. J. Moore, C. C. Fischer, K. A. Persson, and G. Ceder, Formation enthalpies by mixing gga and gga+ u calculations, *Physical Review B—Condensed Matter and Materials Physics* **84**, 045115 (2011).
- [95] V. Stevanović, S. Lany, X. Zhang, and A. Zunger, Correcting density functional theory for accurate predictions of compound enthalpies of formation: Fitted elemental-phase reference energies, *Physical Review B—Condensed Matter and Materials Physics* **85**, 115104 (2012).
- [96] A. Wang, R. Kingsbury, M. McDermott, M. Horton, A. Jain, S. P. Ong, S. Dwaraknath, and K. A. Persson, A framework for quantifying uncertainty in dft energy corrections, *Scientific reports* **11**, 15496 (2021).
- [97] R. S. Kingsbury, A. S. Rosen, A. S. Gupta, J. M. Munro, S. P. Ong, A. Jain, S. Dwaraknath, M. K. Horton, and K. A. Persson, A flexible and scalable scheme for mixing computed formation energies from different levels of theory, *npj Computational Materials* **8**, 195 (2022).
- [98] A. Savin and E. R. Johnson, Judging density-functional approximations: Some pitfalls of statistics, *Density Functionals: Thermochemistry*, 81 (2015).
- [99] J. P. Perdew, J. Sun, A. J. Garza, and G. E. Scuseria, Intensive atomization energy: re-thinking a metric for electronic structure theory methods, *Zeitschrift für Physikalische Chemie* **230**, 737 (2016).
- [100] J. P. Perdew, K. Burke, and M. Ernzerhof, Generalized gradient approximation made simple, *Physical review letters* **77**, 3865 (1996).
- [101] A. Najibi and L. Goerigk, The nonlocal kernel in van der waals density functionals as an additive correction: An extensive analysis with special emphasis on the b97m-v and ω b97m-v approaches, *Journal of Chemical Theory and Computation* **14**, 5725 (2018).
- [102] S. Grimme, J. Antony, S. Ehrlich, and H. Krieg, A consistent and accurate ab initio parametrization of density functional dispersion correction (dft-d) for the 94 elements h-pu, *The Journal of chemical physics* **132** (2010).
- [103] S. Grimme, S. Ehrlich, and L. Goerigk, Effect of the damping function in dispersion corrected density functional theory, *Journal of computational chemistry* **32**, 1456 (2011).
- [104] F. Weigend and R. Ahlrichs, Balanced basis sets of split valence, triple zeta valence and quadruple zeta valence quality for h to rn: Design and assessment of accuracy, *Physical Chemistry Chemical Physics* **7**, 3297 (2005).
- [105] P. J. Stephens, F. J. Devlin, C. F. Chabalowski, and M. J. Frisch, Ab initio calculation of vibrational absorption and circular dichroism spectra using density functional force fields, *The Journal of physical chemistry* **98**, 11623 (1994).
- [106] S.-L. J. Lahey, T. N. Thien Phuc, and C. N. Rowley, Benchmarking force field and the ani neural network potentials for the torsional potential energy surface of biaryl drug fragments, *Journal of Chemical Information and Modeling* **60**, 6258 (2020).
- [107] C. Bannwarth, S. Ehlert, and S. Grimme, Gfn2-xtb—an accurate and broadly parametrized self-consistent tight-binding quantum chemical method with multipole electrostatics and density-dependent dispersion contributions, *Journal of chemical theory and computation* **15**, 1652 (2019).
- [108] J. Riebesell, R. E. A. Goodall, P. Benner, Y. Chiang, B. Deng, A. A. Lee, A. Jain, and K. A. Persson, Matbench discovery – a framework to evaluate machine learning crystal stability predictions (2024), arXiv:2308.14920 [cond-mat.mtrl-sci].
- [109] L. Zhang, J. Han, H. Wang, R. Car, and W. E, Deep potential molecular dynamics: a scalable model with the accuracy of quantum mechanics, *Physical review letters* **120**, 143001 (2018).
- [110] R. Galvelis, A. Varela-Rial, S. Doerr, R. Fino, P. Eastman, T. E. Markland, J. D. Chodera, and G. De Fabritiis, Nnp/mm: accelerating molecular dynamics simulations with machine learning potentials and molecular mechanics, *Journal of chemical information and modeling* **63**, 5701 (2023).
- [111] Y.-L. Liao, B. M. Wood, A. Das, and T. Smidt, Equiformerv2: Improved equivariant transformer for scaling to higher-degree representations, in *The Twelfth International Conference on Learning Representations* (2024).
- [112] H. Kim, J. Y. Park, and S. Choi, Energy refinement and analysis of structures in the qm9 database via a highly accurate quantum chemical method, *Scientific data* **6**, 109 (2019).
- [113] T. W. Ko and S. P. Ong, Data-efficient construction of high-fidelity graph deep learning interatomic potentials (2024), arXiv:2409.00957 [physics.comp-ph].
- [114] B. Deng, Y. Choi, P. Zhong, J. Riebesell, S. Anand, Z. Li, K. Jun, K. A. Persson, and G. Ceder, Overcoming systematic softening in universal machine learning interatomic potentials by fine-tuning (2024), arXiv:2405.07105 [cond-mat.mtrl-sci].
- [115] P. E. Blöchl, Projector augmented-wave method, *Physical review B* **50**, 17953 (1994).

- [116] S. P. Ong, W. D. Richards, A. Jain, G. Hautier, M. Kocher, S. Cholia, D. Gunter, V. L. Chevrier, K. A. Persson, and G. Ceder, Python materials genomics (pymatgen): A robust, open-source python library for materials analysis, *Computational Materials Science* **68**, 314 (2013).
- [117] Y. Qiu, D. G. Smith, C. D. Stern, M. Feng, H. Jang, and L.-P. Wang, Driving torsion scans with wavefront propagation, *The Journal of chemical physics* **152** (2020).
- [118] A. H. Larsen, J. J. Mortensen, J. Blomqvist, I. E. Castelli, R. Christensen, M. Dułak, J. Friis, M. N. Groves, B. Hammer, C. Hargus, *et al.*, The atomic simulation environment—a python library for working with atoms, *Journal of Physics: Condensed Matter* **29**, 273002 (2017).
- [119] P. Eastman, R. Galvelis, R. P. Peláez, C. R. Abreu, S. E. Farr, E. Gallicchio, A. Gorenko, M. M. Henry, F. Hu, J. Huang, *et al.*, Openmm 8: molecular dynamics simulation with machine learning potentials, *The Journal of Physical Chemistry B* **128**, 109 (2023).
- [120] M. J. Abraham, T. Murtola, R. Schulz, S. Páll, J. C. Smith, B. Hess, and E. Lindahl, Gromacs: High performance molecular simulations through multi-level parallelism from laptops to supercomputers, *SoftwareX* **1**, 19 (2015).
- [121] W. L. Jorgensen, J. Chandrasekhar, J. D. Madura, R. W. Impey, and M. L. Klein, Comparison of simple potential functions for simulating liquid water, *The Journal of chemical physics* **79**, 926 (1983).
- [122] J. L. Abascal and C. Vega, A general purpose model for the condensed phases of water: Tip4p/2005, *The Journal of chemical physics* **123** (2005).
- [123] J. V. Valle, B. H. Mendonça, M. C. Barbosa, H. Chacham, and E. E. de Moraes, Accuracy of tip4p/2005 and spc/fw water models, *The Journal of Physical Chemistry B* **128**, 1091 (2024).
- [124] D. Rappoport and F. Furche, Property-optimized gaussian basis sets for molecular response calculations, *The Journal of chemical physics* **133** (2010).
- [125] S. L. Dudarev, G. A. Botton, S. Y. Savrasov, C. Humphreys, and A. P. Sutton, Electron-energy-loss spectra and the structural stability of nickel oxide: An lsda+ u study, *Physical Review B* **57**, 1505 (1998).
- [126] J. Sun, A. Ruzsinszky, and J. P. Perdew, Strongly constrained and appropriately normed semilocal density functional, *Physical review letters* **115**, 036402 (2015).
- [127] J. W. Furness, A. D. Kaplan, J. Ning, J. P. Perdew, and J. Sun, Accurate and numerically efficient r2scan meta-generalized gradient approximation, *The journal of physical chemistry letters* **11**, 8208 (2020).
- [128] L. A. Curtiss, P. C. Redfern, and K. Raghavachari, Gaussian-4 theory, *The Journal of chemical physics* **126** (2007).
- [129] L. A. Curtiss, P. C. Redfern, and K. Raghavachari, Gaussian-4 theory using reduced order perturbation theory, *The Journal of chemical physics* **127** (2007).
- [130] Y. Guo, C. Riplinger, U. Becker, D. G. Liakos, Y. Minenkov, L. Cavallo, and F. Neese, Communication: An improved linear scaling perturbative triples correction for the domain based local pair-natural orbital based singles and doubles coupled cluster method [dlpno-ccsd(t)], *The Journal of chemical physics* **148** (2018).